Journal of Materials Chemistry A

A deeply-rechargeable zinc anode with pomegranate-inspired nanostructure for high-energy aqueous batteries

Journal:	*Journal of Materials Chemistry A*
Manuscript ID	TA-COM-08-2018-007809.R1
Article Type:	Communication
Date Submitted by the Author:	05-Oct-2018
Complete List of Authors:	Chen, Peng; Georgia Institute of Technology, School of Chemical & Biomolecular Engineering; Northeastern University, School of Metallurgy Wu, Yutong; Georgia Institute of Technology, School of Chemical & Biomolecular Engineering Zhang, Yamin; Georgia Institute of Technology, School of Chemical & Biomolecular Engineering Wu, Tzu-Ho; Georgia Institute of Technology, School of Chemical & Biomelecular Engineering Ma, Yao; Georgia Institute of Technology, School of Chemical & Biomolecular Engineering Pelkowski, Chloe; Georgia Institute of Technology, School of Chemical and Biomolecular Engineering Yang, Haochen; Georgia Institute of Technology, School of Chemical & Biomolecular Engineering Zhang, Yi; Georgia Institute of Technology, School of Chemical & Biomolecular Engineering Hu, Xianwei; Northeastern University, School of Metallurgy Liu, Nian; Georgia Institute of Technology, School of Chemical & Biomolecular Engineering

SCHOLARONE™
Manuscripts

A deeply-rechargeable zinc anode with pomegranate-inspired nanostructure for high-energy aqueous batteries

Peng Chen[§,a,b], Yutong Wu[§a], Yamin Zhang[a], Tzuho Wu[a], Yao Ma[a], Chloe Pelkowski[a], Haochen Yang[a], Yi Zhang[a,c], Xianwei Hu[b], Nian Liu[a]*

[a] *School of Chemical and Biomolecular Engineering, Georgia Institute of Technology, Atlanta, GA 30332, USA*

[b] *School of Metallurgy, Northeastern University, Shenyang, Liaoning 110819, China*

[c] *College of Energy and Institute for Electrochemical Energy Storage, Nanjing Tech University, Nanjing, Jiangsu 211816, China*

Email: nian.liu@chbe.gatech.edu

§ The authors contributed equally to this work.

Keywords: aqueous batteries, rechargeable, zinc anode, carbon shell, nanostructure, hierarchical

Abstract

Rechargeable, Zn-based aqueous batteries, because of their advantages of inflammability, high energy density, and low material cost, are an attractive alternative to lithium-ion and lead-acid batteries for transportation and grid-scale applications. Historically, zinc anodes have shown low utilization and rechargeability in alkaline electrolyte due to the entangled problems of ZnO passivation and $Zn(OH)_4^{2-}$ dissolution. Herein, we report a nanoscale, pomegranate-structured Zn anode (Zn-pome), fabricated via a bottom-up microemulsion approach, to overcome these problems. In the Zn-pome, primary ZnO nanoparticles (ZnO NPs) assemble into secondary clusters after which they are individually encapsulated by a conductive, microporous carbon framework. The small size of ZnO NPs overcomes the issue of passivation while the secondary structure and ion-sieving carbon shell mitigate the dissolution problem. Inductively coupled plasma (ICP)

analysis confirmed that Zn dissolution from the Zn-pome anode was effectively suppressed, leading to a considerably prolonged cycle life compared to a conventional ZnO anode in alkaline aqueous electrolyte. The Zn-pome anode even maintains the capacity after long resting. This performance was achieved in harsh yet practical conditions: a limited amount of electrolyte, sealed coin cells, and 100% depth of discharge (DOD). This work represents an important step towards producing aqueous, rechargeable, high-energy batteries. In addition, the design principles reported here are expected to apply to other battery systems involving passivation or dissolution intermediates.

Main text

Depletion of fossil fuel resources is leading to steadily-increasing energy demands. As a result, it is increasingly necessary to develop sustainable electrochemical energy storage (EES) systems that are low-cost, reliable, and eco-friendly.[1–3] Extensive research into EES in recent years has prompted the emergence of crucial technologies for applications in portable devices, electric vehicles (EVs) and grid-scale energy-storage systems.[4–7] Batteries utilizing Faradaic energy storage mechanisms are the most prominent system among the EES technologies.[8,9] Undoubtedly, lithium-ion batteries (LIBs) have been an enormous success in the realms of portable devices and electric vehicles (EVs)[10–12] due to their high energy density, light weight, and low self-discharge rate. For these reasons, Lithium-ion batteries are still receiving much attention.[13,14] However, LIBs continue to face challenges related to safety, energy density, longevity, and concerns around material availability (such as Li and Co metal). Particularly, battery safety is an increasingly vital concern in electric vehicle applications. These issues continue to severely limit the popularization of EVs and the development of grid-energy storage.[15,16] As a solution, fluorinated organic electrolyte[17] and solid-state electrolytes [18–20] are being pursued as alternatives to flammable organic

solvents. Another approach towards ultra-safe batteries is to develop battery chemistries that are compatible with aqueous electrolytes.[21–23] The main obstacles for aqueous batteries include their narrow stable voltage window and the evolution of hydrogen and oxygen gas that occurs with the electrolysis of water.[24–26] Thus, the need for ultra-safe, high-energy, and low-cost electrochemical energy storage devices has prompted a search for new energy storage technologies.

Rechargeable Zn-based aqueous batteries have immense potential in large-scale energy storage systems due to their high capacity (820 $Ah \cdot kg^{-1}$ and 5854 $Ah \cdot L^{-1}$), cost-effectiveness, and high chemical stability in air and aqueous solution.[27–31] Without the necessity of flammable organic electrolyte, aqueous Zn-based batteries will not require the comparably complex subsystems required for lithium-based batteries, including thermal management, sophisticated electronic controls, and structural protection to manage any catastrophic events.[32,33] In contrast to a LIB graphite host anode, which undergoes intercalation and de-intercalation, the zinc anode undergoes dissolution/precipitation, complexation, and reduction/oxidation repetitive processes during the charge/discharge process in aqueous electrolyte. The overall reactions on the zinc anode are shown in equations 1, 2 and 3:

$$ZnO\ (s) + H_2O\ (l) + 2OH^-\ (aq) \rightleftharpoons Zn(OH)_4^{2-}\ (aq) \quad (1)$$

$$Zn(OH)_4^{2-}\ (aq) + 2e^- \rightleftharpoons Zn\ (s) + 4OH^-\ (aq) \quad (2)$$

$$\text{Overall: } ZnO\ (s) + H_2O\ (l) + 2e^- \rightleftharpoons Zn\ (s) + 2OH^-\ (aq) \quad (3)$$

As a result of this dissolution/precipitation cycle, the long-standing constraint that has prevented the implementation of Zn in next-generation batteries for large-scale application is its poor rechargeability due to dendrite growth, shape change, and passivation.[34] Zn dendrites are formed during the charging process (i.e., electrodeposition of Zn metal) when $Zn(OH)_4^{2-}$ and/or Zn^{2+} ions are deposited unevenly, with faster growth occurring along energetically favorable crystallographic directions, resulting in internal short circuit. Furthermore, incomplete reduction of

zincate ions coupled with non-uniform redistribution of Zn electrode material during the charging process leads to densification of the electrode at specific regions over many charge/discharge cycles, causing loss of usable capacity. Aside from dendrite formation and shape change of the Zn electrode, the passivation layer on the bulk zinc anode shortens the cycle life because active Zn is transformed into relatively insulating ZnO, which increases the internal resistance of the Zn electrode. This passivation inhibits the discharge process as the insulating ZnO film on the Zn surface blocks migration of the discharge products and/or hydroxide ions, causing significant loss of energy efficiency for the charge/discharge cycles. In past decades, the passivation mechanism of Zn anode in alkali electrolyte has been widely investigated.[35–37] However, effective methods of resolving this problem have yet to be proposed.

Recently, attempts have been made to mitigate dendrite formation and shape change of the Zn electrode by altering the Zn electrode design.[38] A 3D-zinc sponge anode was prepared to improve the rechargeability of Zn-based batteries.[39,40] Although the performance of the zinc battery was improved dramatically with this design, there are still problems in the proposed Zn electrode: 1) passivation is still present in the 3D-zinc anodes, especially with high DOD; 2) the larger electrode-electrolyte contact area accelerates the dissolution of zinc, leading to shape change and capacity fade; and 3) the volume capacity decreased because of the porosity of the zinc sponge and the low depth-of-discharge. In another investigation, Zn anodes with a carbon coating were utilized to improve anti-corrosion performance.[41–43] Unfortunately, however, most of these works were not able to overcome the dissolution and passivation problems simultaneously. In these works, although nanoscale, carbon-coated zinc oxide particles were used as the anode material in rechargeable zinc cells, there is considerable room for improvement to mitigate the dissolution problem. An anode composed of micron-sized ZnO spheres was synthesized by a complicated co-precipitation process or ball milling approach, which increases the tap density of the electrode, but

the passivation problem still needs to be resolved[44]. Also, some zinc battery systems using mild electrolyte, such as $ZnSO_4$-MSO_4(M=Mn, Co)[45,46], and $Zn(CF_3SO_3)_2$-$Mn(CF_3SO_3)$[47], $Zn(TFSI)_2$-LiTFSI[48] in which the expensive TFSI salts should be replaced with lower cost salts, were developed to mitigate the zinc dendritic growth effectively. Nevertheless, the reversibility of zinc anode in alkaline electrolyte is receiving a great of concern to exploit some highly rechargeable Zn-air batteries with high specific energy density (5200 $Wh•Kg^{-1}$)[49].

In terms of battery testing protocols, most past reports of Zn anode performance were obtained in beaker cells rather than closed cells (cylindrical cells or coin cells) [38,41,42,50]. In these beaker cells, the plentiful electrolyte significantly decreased the overall specific capacity of batteries. Also, since electrolyte saturated with ZnO was used in these beaker cells, it is difficult to attribute the contribution of active material and calculate the performance of batteries due to the inevitable reduction of zincate from outsourcing of ZnO in the electrolyte. The performance of these cells cannot reflect real conditions in practical commercial batteries in which the reasonable electrolyte content is a pivotal factor for high volumetric and gravimetric capacity.

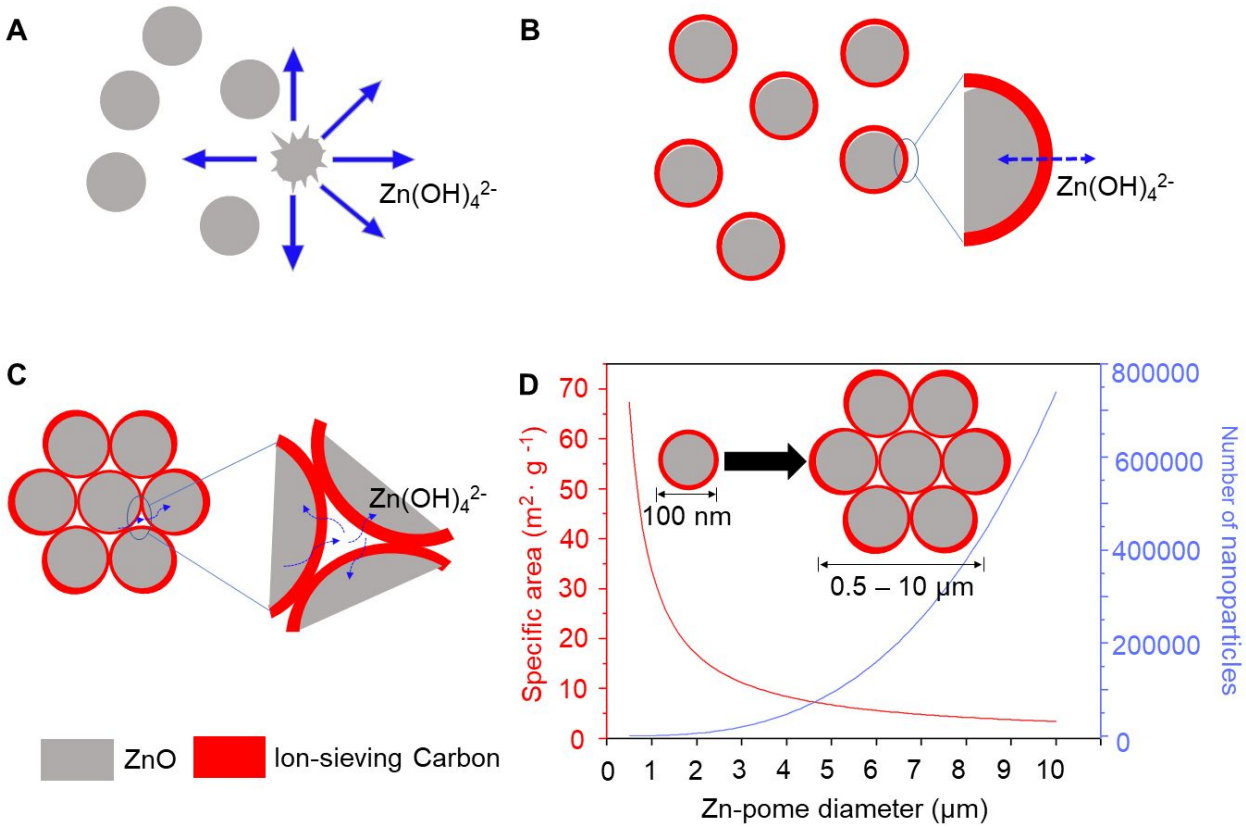

Fig. 1 Cross section schematic of the Zinc pomegranate design. A) ZnO NPs with fast dissolution rate in alkaline aqueous solution; B) ZnO NPs coated with carbon; C) Zn-pomegranate in which carbon filled into the free space of ZnO clusters plays a crucial role in ion sieving, conductivity, and structure stabilization of the electrode; D) Calculated surface area in contact with electrolyte and the number of primary nanoparticles in one Zn pomegranate cluster versus its diameter. The smaller the surface contact with the electrolyte, the lower capacity fading.

To tackle the long-standing challenges of a completely rechargeable Zn anode in a limited quantity of electrolyte, we designed a ZnO pomegranate (Zn-pome) material in which the zinc oxide nanoparticles (ZnO NPs) are analogous to *seeds* that are individually encapsulated and held in clusters by a carbon shell diaphragm. The carbon shell coating on the nanoparticles was chosen for its porosity, stability in aqueous alkaline media, and electroconductivity. **Fig. 1A** shows the schematic of zincate motion during battery cycling of ZnO NPs (**Fig. 1A**), ZnO@C NPs (**Fig. 1B**)

and Zn-pome (**Fig. 1C**), respectively. There are several distinctive advantages to the Zn-pome electrode. First, the multi-layered carbon acts as a conductor, protector, and ion barrier in Zn-pome to adequately constrain the migration of the $Zn(OH)_4^{2-}$ (the discharge product), thus mitigating the dendrite formation and shape change of the Zn electrode. Meanwhile, species with a smaller diameter (e.g. OH^- and H_2O) than that of zincate can permeate through the carbon shell. Second, the use of nanoscale (< 100 nm) primary ZnO particle avoids passivation. Once ZnO reaches a critical passivation thickness, it can no longer fully convert to Zn. The thickness of the passivation layer on zinc foil in coin cells after fully discharging was determined by scanning electron microscope (SEM). As shown in **Fig. S1** (EIS†), the feature thickness of the passivation layer is ca. 2 μm, which indicates that the Zn anode cannot be consumed entirely in the discharge process if the size of the Zn material is larger than ca. 2 μm regardless of the shape (foil, rod or particle, etc.). Thus, controlling the size of Zn material to nanoscale is a practical approach to fully utilize the Zn material in the charge/discharge process. Therefore, the nanoscale ZnO primary material was chosen to build the Zn-pome. Besides, the robust carbon shell on ZnO NPs is both electrically and ionically conducting, which not only allows for good kinetics, but also improves the mechanical strength of the Zn anode. Third, the Zn-pome has a smaller solid-electrolyte contact area than ZnO@C NPs (As shown in **Fig. 1D**), which can significantly reduce the dissolution rate during cycling. Hence, the long-standing limits that have impeded the rechargeability of Zn electrode (i.e., Zn dendrite formation, Zn electrode shape change and ZnO passivation) can be significantly alleviated by the electrode design of Zn-pome.

The synthesis of Zn-pome is schematically illustrated in **Fig. S2** (ESI†). Micro-emulsion procedures have been used to synthesize other electrode materials with hierarchical particulate structures, for application in LIB[51] and Li-S battery[52]. In this work, ZnO NPs were first dispersed in distilled water by ultrasonication and then mixed with 1-octadecene solution containing

emulsion stabilizer. After removing the water and organics, the ZnO NPs self-assembled to form close-packed ZnO clusters and were then condensed by calcined (**Fig. S2A,** ESI†). The obtained clusters were subsequently coated with a thin layer of dopamine, which was further carbonized under argon atmosphere to form Zn-pome.

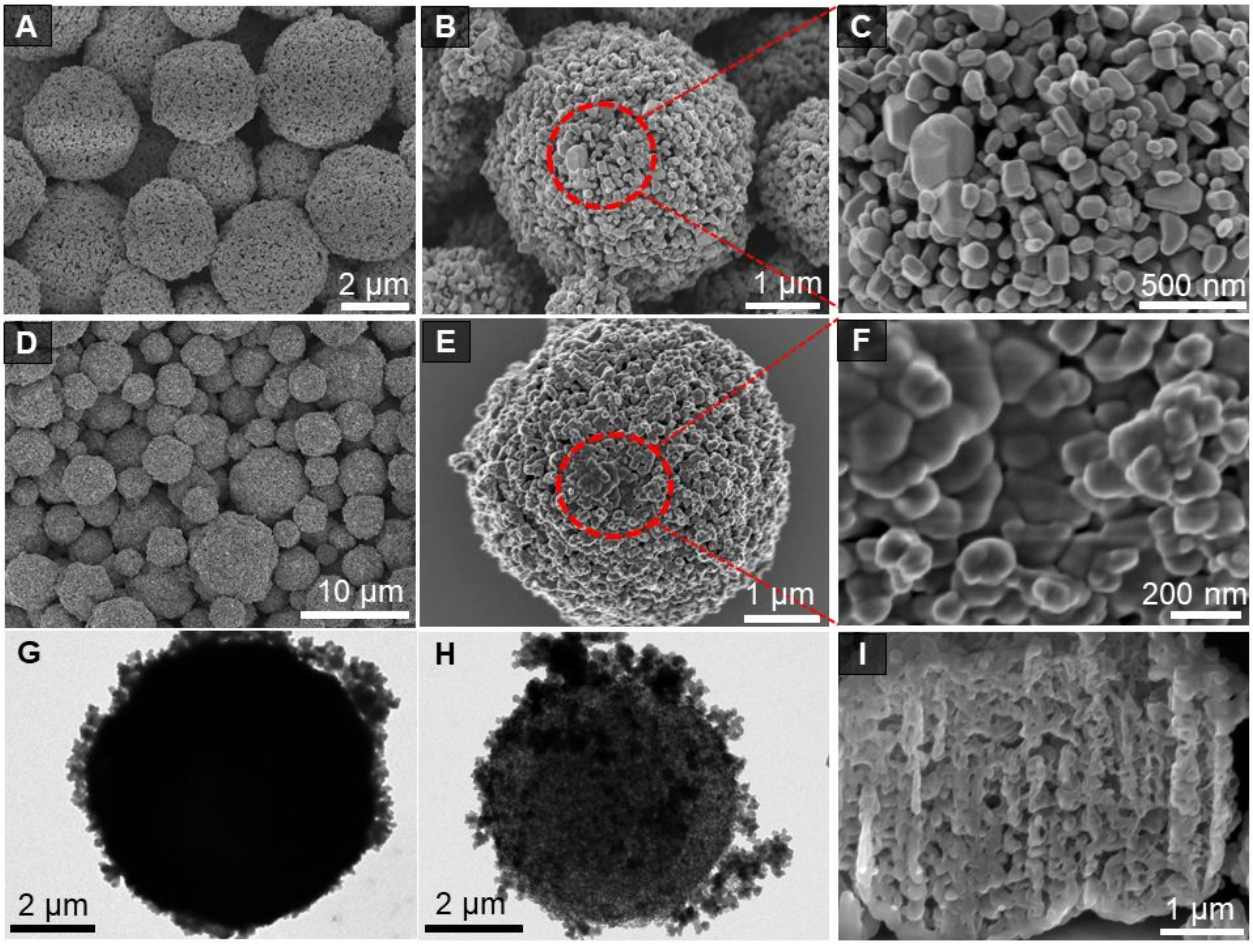

Fig. 2 (**A-C**) SEM images of clusters of ZnO nanoparticles assembled via a microemulsion approach. (**D-F**) SEM images of Zn-pome (nanoporous carbon coated ZnO cluster). (**G**) TEM image of Zn-pome. (**H**) TEM image of the carbon framework of Zn-pome after etching away ZnO in 1 M HCl for 24 hours. (**I**) Cross-sectional SEM image of one Zn-pome microparticle obtained by focused ion beam (FIB) analysis.

The SEM images of the ZnO clusters were investigated under various magnifications (**Fig. 2A-C**). These clusters with diameters in the range of 1-6 μm consisting of primary ZnO NPs. The

rounded edge of the Zn-pome (**Fig. 2D-F**) indicates that the ZnO clusters were adequately coated with a thin layer of carbon framework. The detailed structure of the Zn-pome was investigated using higher resolution transmission electron microscope (HRTEM) and focus ion beam milling image (FIB) analysis. According to the TEM images (**Fig. 2G** and **Fig. S3A,** ESI†), the diameter of a typical Zn-pome microparticle is ca. 6 μm. When the Zn-pome was treated with 1M HCl to etch away ZnO, the hollow carbon framework can be clearly observed in TEM images (**Fig. 2H** and **Fig. S3C-F,** ESI†). This indicates each of the ZnO NPs was individually coated by a thin layer of carbon framework with the thickness of ca. 10-15 nm. Moreover, the coated carbon framework is stable even without the solid "seeds", ZnO NPs, which is crucial for the structural stability of the Zn-pome especially when the active Zn material is mainly oxidized and dissolved after deep discharge process. **Fig. 2I** exhibits the cross-sectional images of the Zn-pome microparticle obtained by the Focus Ion Beam milling image (FIB) analysis. A secondary Zn-pome microparticle consists of ZnO NPs clusters, in which each of ZnO NPs, with rounded surface, was uniformly capsuled by the carbon framework. More cross-sectional images are illustrated in **Fig. S4** (ESI†). The abovementioned morphology investigations of Zn-pome reveal that the Zn-pome fabricated by bottom-up approach, consisting of robust carbon framework and ZnO nanoparticles, can be used to anode in zinc-based batteries.

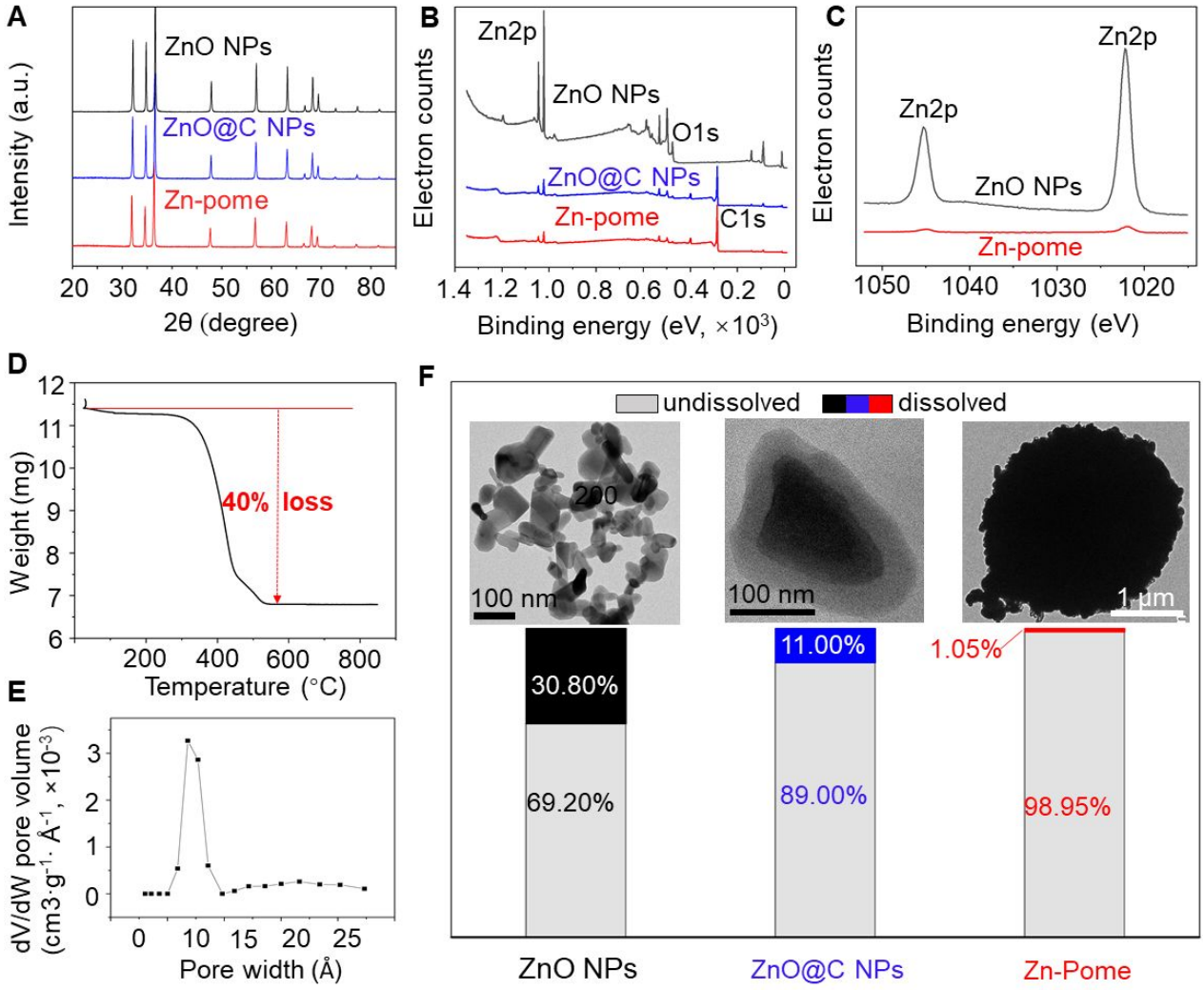

Fig. 3 (A) XRD patterns and (**B**) XPS spectra of ZnO NPs, ZnO@C NPs and Zn-pome. (**C**) High-resolution XPS spectra of ZnO NPs and Zn-pome. **(D)** TGA weight loss curve and (**E**) BET pore size distribution of Zn-pome. (**F**) Dissolved and undissolved portions of zinc in 4 M KOH electrolyte for ZnO NPs, ZnO@C NPs and Zn-pome, embedded pictures show the electron microscopic images of ZnO NPs, ZnO@C NPs and Zn-pome.

X-ray diffraction (XRD) and X-ray photoelectron spectroscopy (XPS) were used to characterize the crystal structure and chemical composition of Zn-pome (**Fig. 3A-C**). The XRD pattern of the Zn-pome is similar to that of the ZnO NPs and ZnO@C NPs. No characteristic peak of carbon was detectable, indicating an amorphous coating of carbon on the ZnO NPs. The reduced

intensity of ZnO for Zn-pome suggests the ZnO NPs are uniformly covered by the carbon framework, therefore, it shields the diffractive signals of ZnO slightly. Similarly, strong C1s signal and relatively weak Zn2p and O1s signals in the XPS survey spectrum can be observed for Zn-pome in comparison with ZnO NPs. Accordingly, the Zn-pome is characterized as the ZnO NPs clusters uniformly coated with an amorphous carbon layer. The content of carbon is found to be about 40% in the Zn-pome based on thermogravimetric analysis (TGA) in air, as shown in **Fig. 3D**. The Brunauer-Emmett-Teller (BET) result reveal that the average pore size of the carbon shell is ca. 10 Å (**Fig. 3E**). This indicates the carbon framework can properly mitigate the permeation of zincate through the shell structure.

In order to verify the ion-sieving ability of the carbon coating, we investigated the dissolution rate of the ZnO in aqueous alkaline electrolyte. Samples of ZnO NPs, ZnO@C NPs and Zn-pome containing equal amount of zinc were immersed in 1 mL of 4 M KOH solutions at the same time, respectively. After a certain amount of time, the concentration of Zn species dissolved in the solutions were analyzed by inductively coupled plasma (ICP). As shown in **Fig. 3F**, the Zn-pome significantly reduces the portion of dissolved Zn in KOH (1.05%) in comparison with ZnO NPs (30.8%) and ZnO@C NPs (11%). This effect is attributed to the synergistic function of carbon shell and secondary structure in Zn-pome. The diffusion of zincate in alkaline media is confined within the secondary particle, while the confined zincate can still be electrochemically reduced. The pomegranate structure is also expected to alleviate the Zn dendrite formation and shape change (i.e., localized densification) during charge/discharge process. Thus, the long-standing constrains for rechargeability of Zn electrodes can be effectively overcome.

The electrochemical performance of the Zn-pome and ZnO NPs was evaluated by a full cell configuration consisting of $Ni(OH)_2$ cathode with excess capacity obtained from commercial zinc-nickel batteries. The cells were cycled at 1 C in a voltage window between 1.5 and 2.0 V in 2 M

KF, 2 M K_2CO_3 and 4 M KOH.[53] It should be noted that the battery testing protocols used in this work were extremely harsh in three aspects: 1) Lean electrolyte. We used 2032 coin cells with a limited amount of electrolyte (**Fig. S5,** ESI†) rather than beaker cell with excess electrolyte because coin cells better represent real operating conditions. 2) ZnO-free electrolyte. ZnO-saturated KOH electrolyte is commonly used to provide higher specific capacity and longer cycle life, but zinc species initially present in the electrolyte are likely to contribute to the capacity of the cell and conceal the actual performance of active zinc material on the electrode. 3) 100% depth of discharge (DOD). Under 100% DOD, the full energy density can be delivered. Generally, however, <50% DOD is used for Zn anodes because of the passivation problem.

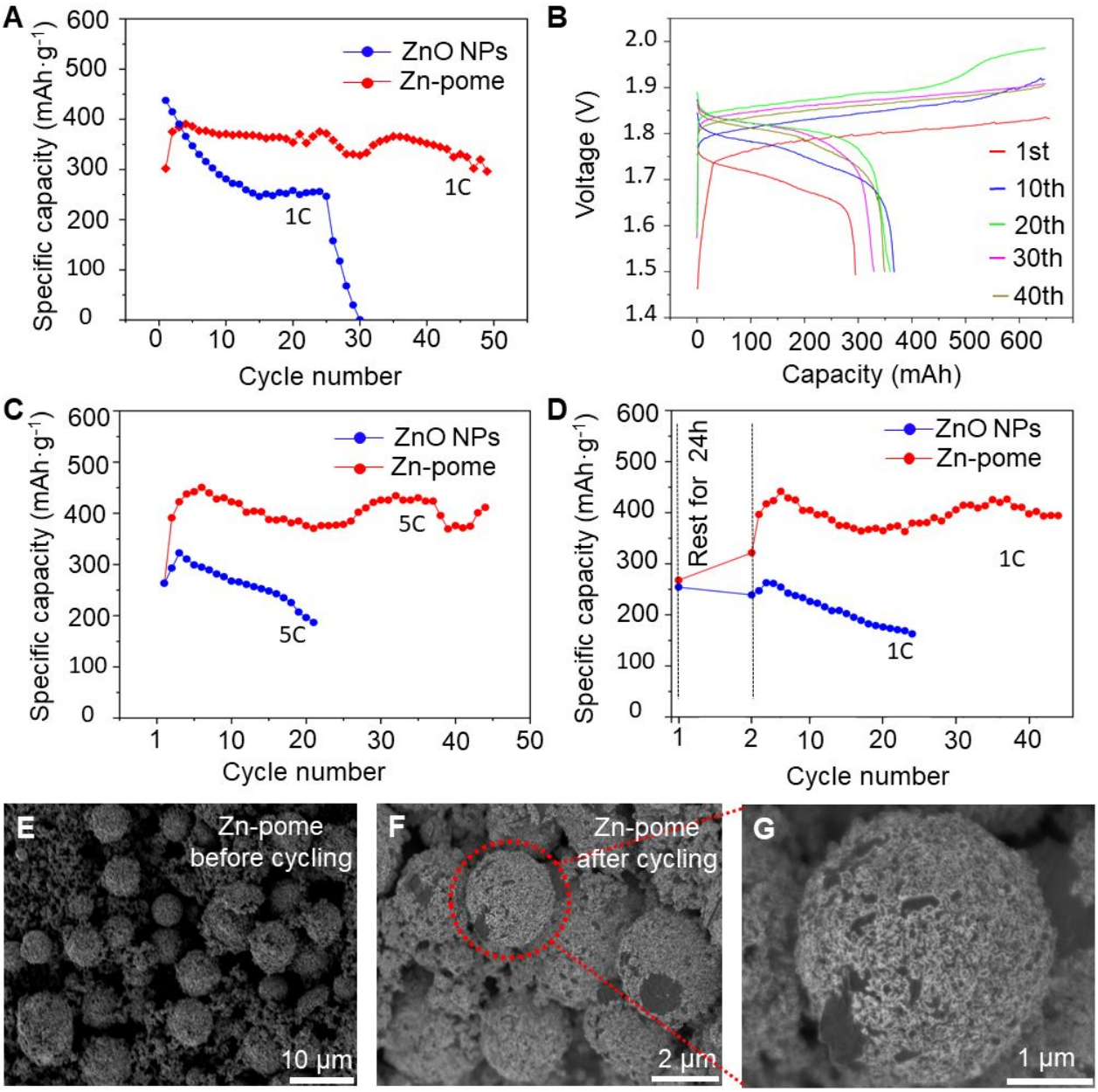

Fig. 4. (**A**) Specific capacity of ZnO NPs and Zn-Pome. (**B**) Voltage profiles of Zn-Pome/$Ni(OH)_2$. (**C**) Specific capacity of ZnO NPs/$Ni(OH)_2$ and Zn-Pome/$Ni(OH)_2$ at 5C discharge rate. (**D**) Testing of self-discharge of Zn-pome cells cycling at 0.5 C for one cycle, resting for 24 h, then cycling at 1 C. (**E**) SEM image of Zn-pome anode before cycling (**F** and **G**) and. after two cycles.

Under such harsh testing condition, the cells containing the Zn-pome anode (Zn-pome/$Ni(OH)_2$) exhibited a remarkable capacity and cycle life, superior to that of the ZnO NPs and

ZnO NPs@C anode with $Ni(OH)_2$ cathode repectively. As shown in **Fig. 4A** and **Fig. S6** (ESI†), although the specific capacity of the Zn NPs/$Ni(OH)_2$ was higher than that of Zn-pome in the first few cycles, the discharge capacity of the Zn NPs/$Ni(OH)_2$ decreased sharply over 20 cycles due to the fading of the anode resulting from high dissolution rate of ZnO in strong aqueous alkali electrolyte. The problem of abrupt capacity decay of the control sample after 25 cycles can best be attributed to high dissolution of zinc, which subsequently results in the formation of dendrites, as well as substantial electrode shape change after several cycles from repeated redistribution of active material. Other issues stem from the hydrogen evolution reaction (HER) on the surface of the zinc, which not only worsens the efficient utilization of the zinc but also leads to swelling of the cell, causing the cell to crack and the electrolyte to dry out. The loose contact in the cells inflated by hydrogen further cause abrupt capacity fading. In contrast, the capacity of the Zn-pome/$Ni(OH)_2$ was stable for 50 cycles and then gradually decreased, showing a better cyclability than the Zn NPs/$Ni(OH)_2$. This improvement could be attributed to the ion blocking ability of the carbon shell in the Zn-pome anode and the smaller solid-electrolyte contact area. **Fig. 4B** presents the typical charge/discharge profiles of the Zn-pome/$Ni(OH)_2$ battery in the 1^{st}, 10^{th}, 20^{th}, 30^{th} and 40^{th} cycles. The average discharge voltage of the Zn-pome/$Ni(OH)_2$ cell maintained at 1.80 V after 40 cycles, indicating excellent cycling stability.

The improved performance of the Zn-pome/$Ni(OH)_2$ cells compared to Zn NPs/$Ni(OH)_2$ is attributed to the ion-sieving ability of the carbon shell and secondary particle structure. The increase in charging voltage in consecutive cycling is likely due to the accummlation of hydrogen evolved in the reduction of water. Although managing gas generation in sealed cells remains a concern, the hydrogen evolution can be effectively suppressed by the adjustments of electrolyte (such as the use of water-in-salt[48]or solid state additives[54–56]). This work mainly focuses on the structure design of Zn anode.

The electrochemical performance of the Zn-pome/$Ni(OH)_2$ is also superior to the Zn NPs/$Ni(OH)_2$ at a higher discharge rate (5 C), as shown in **Fig. 4C** and **Fig. S7** (ESI†). The discharge capacity of the Zn-pome/$Ni(OH)_2$ maintained around 400 $mAhg^{-1}$ for 45 cycles (e.g. 411 $mAhg^{-1}$ at the 44^{th} cycle). However, the Zn NPs/$Ni(OH)_2$ suffers from a quick decay of discharge capacity after the 3^{rd} cycle (merely 186 $mAhg^{-1}$ at the 21^{st} cycle). Accordingly, the superior performance (both specific capacity and cyclability) of Zn-pome in comparison with ZnO NPs clearly demonstrate the merits of nano-design of pomengranate-structure ZnO.

To further investigate the dissolution-resistivity, the coin cells were conducted one cycle at 0.5 C and then rested for 24 hours before resumed cycling at 1 C. During the 24-hr resting, the Zn anodes are in the discharged state, and ZnO, the dominant species, would rapidly dissolve in electrolyte if left unprotected (see **Fig. 3F**). As shown in **Fig. 4D** and **Fig. S8** (ESI†), the Zn NPs/$Ni(OH)_2$has fast capacity fading. On the other hand, the Zn-pome/$Ni(OH)_2$ still exhibits high capacity after resting and maintains 84% of capacity even after 40 cycles (on the basis of the 3^{rd} cycle), indicating that Zn-pome anode is effective in retaining the Zn active species due to the carbon framework. The morphology evolution of Zn-pome was investigated by SEM (**Figs. 4E-4G, and Fig. S9 (**ESI†)). The Zn-pome anode maintained the microspheric morphology after ten charge/discharge cycles, indicating the robust morphology of the pomegranate structure. Therefore, the Zn-pome is considered to be a novel Zn anode material that can mitigate the Zn dendrtie formation, shape change and passivation issues in alkaline Zn ion batteries.

In summary, we have designed and synthesized a nanoscale pomegranate-inspired hierarchical Zn anode material (Zn-pome) via a bottom-up microemulsion approach. Each Zn-pome microsphere is around 6 μm composed of ~10^5 ZnO nanoparticles individually encapsulated by an amorphous, micropourous, and conductive carbon shell that slows down the dissolution of zincate intermediate species during cycling. The secondary structure further suppresses the zinc

dissolution by decreasing the electrode-electrolyte contact area. ICP analysis confirms that Zn-pome has significantly suppressed dissolution of zinc compared to ZnO NPs nanoparticles and ZnO@C nanoparticles. Because of this design, the Zn-pome anode demonstrated remarkable capacity and cycle stability under extremely harsh testing conditions (lean electrolyte, ZnO-free electrolyte, 100% DOD). It also retained high capacity after long-term resting in a discharged state, in which the ZnO in the electrode has a massive tendency to dissolve. The success of the Zn-pome anode can be attributed to a few design principles that manage soluble intermediates during repeated electrochemical cycling, which is essential for the future design of Zn aqueous anodes as well as other battery systems involving soluble intermediates (e.g., lithium-sulfur batteries).

Experiment section

Detailed experimental methods can be found in the supporting information.

Acknowledgments

The work was financially supported by faculty startup fund from Georgia Institute of Technology. Material characterization was performed in part at the Georgia Tech Institute for Electronics and Nanotechnology, a member of the National Nanotechnology Coordinated Infrastructure, which is supported by the National Science Foundation (Grant ECCS-1542174). We also acknowledge the support of the China Scholarship Council (201706080048) and Ministry of Science and Technology (107-2917-I-564-040).

References

1 M.-C. Lin, M. Gong, B. Lu, Y. Wu, D.-Y. Wang, M. Guan, M. Angell, C. Chen, J. Yang, B.-J. Hwang and H. Dai, *Nature*, 2015, **520**, 324–328.

2 J. Sun, H. Lee, M. Pasta, Y. Sun, W. Liu and Y. Li, *Energy Storage Mater.*, 2016,

4, 130–136.

3 S. Chu, Y. Cui and N. Liu, *Nature*, 2017, **16**, 16–22.

4 B. Dunn, H. Kamath and J.-M. Tarascon, *Science (80-.).*, 2011, **334**, 928–935.

5 S. A. Freunberger, *Nat. Energy*, 2017, **2**, 17091.

6 G. He, Q. Chen, P. Moutis, S. Kar and J. F. Whitacre, *Nat. Energy*, 2018, **3**, 404–412.

7 Y. Gogotsi and P. Simon, *Science (80-.).*, 2011, **334**, 917–918.

8 P. Simon, Y. Gogotsi and D. Bruce, *Science (80-.).*, 2014, **343**, 1210–1212.

9 M. Pasta, C. D. Wessells, R. A. Huggins and Y. Cui, *Nat. Commun.*, 2012, **3**, 1147–1149.

10 J. M. Tarascon and M. Armand, *Nature*, 2001, **414**, 359–367.

11 D. Lin, Y. Liu and Y. Cui, *Nat. Nanotechnol.*, 2017, **12**, 194–206.

12 L. Zhou, X. Zhou, X. Huang, Z. Liu, D. Zhao, X. Yao and C. Yu, *J. Mater. Chem. A*, 2013, **1**, 837–842.

13 Q. Shi, Y. Zhong, M. Wu, H. Wang and H. Wang, *Proc. Natl. Acad. Sci.*, 2018, 1–5.

14 Y. Zhang, Y. Jiang, Y. Li, B. Li, Z. Li and C. Niu, *J. Power Sources*, 2015, **281**, 425–431.

15 P. Albertus, S. Babinec, S. Litzelman and A. Newman, *Nat. Energy*, 2018, **3**, 16–21.

16 K. Liu, Y. Liu, D. Lin, A. Pei and Y. Cui, *Sci. Adv.*, 2018, **4**, eaas9820.

17 X. Fan, L. Chen, O. Borodin, X. Ji, J. Chen, S. Hou, T. Deng, J. Zheng, C. Yang, S.-C. Liou, K. Amine, K. Xu and C. Wang, *Nat. Nanotechnol.*, 2018, **13**, 715–722.

18 L. Fan, S. Wei, S. Li, Q. Li and Y. Lu, *Adv. Energy Mater.*, 2018, **1702657**, 1–31.

19 L. Yang, Z. Wang, Y. Feng, R. Tan, Y. Zuo, R. Gao, Y. Zhao, L. Han, Z. Wang and F. Pan, *Adv. Energy Mater.*, 2017, **7**, 1–9.

20 X. Han, Y. Gong, K. Fu, X. He, G. T. Hitz, J. Dai, A. Pearse, B. Liu, H. Wang, G. Rubloff, Y. Mo, V. Thangadurai, E. D. Wachsman and L. Hu, *Nat. Mater.*, 2017, **16**, 572–579.

21 R. Malik, *Joule*, 2017, **1**, 17–19.

22 Z. Chang, C. Li, Y. Wang, B. Chen, L. Fu, Y. Zhu, L. Zhang, Y. Wu and W. Huang, *Sci. Rep.*, 2016, **6**, 2–7.

23 Y. Liang, Y. Jing, S. Gheytani, K. Y. Lee, P. Liu, A. Facchetti and Y. Yao, *Nat. Mater.*, 2017, **16**, 841–848.

24 L. Suo, O. Borodin, T. Gao, M. Olguin, J. Ho, X. Fan, C. Luo, C. Wang and K. Xu, *Science (80-.).*, 2015, **350**, 938–943.

25 H. Kim, J. Hong, K. Y. Park, H. Kim, S. W. Kim and K. Kang, *Chem. Rev.*, 2014, **114**, 11788–11827.

26 J. Y. Luo, W. J. Cui, P. He and Y. Y. Xia, *Nat. Chem.*, 2010, **2**, 760–765.

27 Y. Li and H. Dai, *Chem. Soc. Rev.*, 2014, **43**, 5257–5275.

28 Y. Li, M. Gong, Y. Liang, J. Feng, J. E. Kim, H. Wang, G. Hong, B. Zhang and H. Dai, *Nat. Commun.*, 2013, **4**, 1805–1807.

29 J. S. Lee, S. T. Kim, R. Cao, N. S. Choi, M. Liu, K. T. Lee and J. Cho, *Adv. Energy Mater.*, 2011, **1**, 34–50.

30 D. E. Turney, J. W. Gallaway, G. G. Yadav, R. Ramirez, M. Nyce, S. Banerjee, Y. C. K. Chen-Wiegart, J. Wang, M. J. D'Ambrose, S. Kolhekar, J. Huang and X. Wei, *Chem. Mater.*, 2017, **29**, 4819–4832.

31 Y. Zhang and N. Liu, *Chem. Mater.*, 2017, **29**, 9589–9604.

32 D. Kundu, B. D. Adams, V. Du, S. H. Vajargah and L. F. Nazar, *Nat. Energy*, 2016, **1**, 1–8.

33 Y. Sun, N. Liu and Y. Cui, *Nat. Energy*, 2016, **1**, 16071.

34 J. Fu, Z. P. Cano, M. G. Park, A. Yu, M. Fowler and Z. Chen, *Adv. Mater.*, 2017, **29**, 1604685.

35 M.-B. Liu, *J. Electrochem. Soc.*, 1981, **128**, 1663.

36 R. W. Powers and M. W. Breiter, *J. Electrochem. Soc.*, 1969, **116**, 719.

37 M. Bockelmann, L. Reining, U. Kunz and T. Turek, *Electrochim. Acta*, 2017, **237**, 276–298.

38 S. Higashi, S. W. Lee, J. S. Lee, K. Takechi and Y. Cui, *Nat. Commun.*, 2016, **7**, 1–6.

39 J. F. Parker, C. N. Chervin, I. R. Pala, M. Machler, M. F. Burz, J. W. Long and D. R. Rolison, *Science (80-.).*, 2017, **356**, 415–418.

40 J. F. Parker, C. N. Chervin, E. S. Nelson, D. R. Rolison and J. W. Long, *Energy Environ. Sci.*, 2014, **7**, 1117–1124.

41 Z. Feng, Z. Yang, J. Huang, X. Xie and Z. Zhang, *J. Power Sources*, 2015, **276**, 162–169.

42 W. Long, Z. Yang, X. Fan, B. Yang, Z. Zhao and J. Jing, *Electrochim. Acta*, 2013, **105**, 40–46.

43 C. Yang, Z. Zhang, Z. Tian, K. Zhang, J. Li and Y. Lai, *Mater. Lett.*, 2017, **197**, 163–166.

44 T. Zhao, E. Shangguan, Y. Li, J. Li, Z. Chang, Q. Li, X. Z. Yuan and H. Wang, *Electrochim. Acta*, 2015, **182**, 173–182.

45 H. Pan, Y. Shao, P. Yan, Y. Cheng, K. S. Han, Z. Nie, C. Wang, J. Yang, X. Li, P.

Bhattacharya, K. T. Mueller and J. Liu, *Nat. Energy*, 2016, **1**, 1–7.

46 L. Ma, S. Chen, H. Li, Z. Ruan, Z. Tang, Z. Liu, Z. Wang, Y. Huang, Z. Pei, J. A. Zapien and C. Zhi, *Energy Environ. Sci.*, , DOI:10.1039/C8EE01415A.

47 N. Zhang, F. Cheng, J. Liu, L. Wang, X. Long, X. Liu, F. Li and J. Chen, *Nat. Commun.*, 2017, **8**, 1–9.

48 F. Wang, O. Borodin, T. Gao, X. Fan, W. Sun, F. Han, A. Faraone, J. A. Dura, K. Xu and C. Wang, *Nat. Mater.*, 2018, **17**, 543–549.

49 P. Gu, M. Zheng, Q. Zhao, X. Xiao, H. Xue and H. Pang, *J. Mater. Chem. A*, 2017, **5**, 7651–7666.

50 B. S. Kwak, S. W. Jo, K. S. Park, T. W. Cho, J. Jeon, K. il Chung and M. Kang, *J. Ind. Eng. Chem.*, 2017, **46**, 111–118.

51 N. Liu, Z. Lu, J. Zhao, M. T. Mcdowell, H. W. Lee, W. Zhao and Y. Cui, *Nat. Nanotechnol.*, 2014, **9**, 187–192.

52 W. Li, Z. Liang, Z. Lu, H. Yao, Z. W. Seh, K. Yan, G. Zheng and Y. Cui, *Adv. Energy Mater.*, 2015, **5**, 1500211.

53 P. Bonnick and J. R. Dahn, *J. Electrochem. Soc.*, 2012, **159**, A981–A989.

54 J. Mcbreen and E. Gannon, *J. Power Sources*, 1985, **15**, 169–177.

55 R. Shivkumar, G. P. Kalaignan and T. Vasudevan, *J. Power Sources*, 1998, **75**, 90–100.

56 A. Renuka, A. Veluchamy, N. Venkatakrishnan and S. N. Beoum, *J. Appl. Electrochem.*, 1992, **22**, 22–24.